Simulating Electrochemical Reactions

Rui Fang and Martin Jin

05/11/2018

Abstract

In this project, we simulate the one-electron electrochemical process in cyclic voltammetry (CV) experiments, a system described by the diffusion equation subject to time-dependent boundary conditions. We compare the accuracy and efficiency of several implicit finite difference methods and two different linear system solvers. Using the most accurate and efficient method, we examine the effects of various parameters on the CV simulations, such as the kinetic constant and charge transfer coefficient. Lastly, we compare an experimental CV with several simulated CVs and illustrate how simulations can help us infer properties of the electrochemical reaction.

Introduction

The study of electrochemistry began in the late seventeen hundreds, when Luigi Galvani's claim of the existence "animal electricity" first time linked the two scientific fields, chemistry and electricity, together. Although "animal electricity" was found to be a false concept, later discoveries such as Alessandro Volta's electric-current metal pile and William Nicholson's water electrolysis pointed out that chemical reactions can generate electricity and electricity can provide driving force for chemical reactions. Nowadays, electrochemistry is the foundation of many heavily industry-related fields, such as metal-plating, corrosion and energy[1].

Battery is among the commonest goods and the hottest research fields. The quality of a battery material is heavily determined by its chemical and transport properties, which are often characterized by electrochemical methods. However, to accurately determine the properties such as electron-transfer kinetic rate constant, diffusion coefficient, surface area of an electrode and charge transfer coefficient, one needs to take multiple data with changing variables and repeat the experiments multiple times for statistical consistency. The whole procedure may take days and weeks. Numerical simulation of electrochemical processes can reduce the amount of wet lab work while providing a clear image of the behavior of a material [2][1].

This project aims to simulate cyclic voltammetry (CV), one of the simplest but most used techniques in electrochemical analyses. A typical one-electron reversible process looks like figure 1a. In a CV process, the electrode is immersed in a solution full of species O, and the electrode potential (E) is swept linearly with time and swept backward at a manually set value(see figure 1b). Once the electrode potential reaches a level where species O is no longer stable, the reduction of O to a different species R will occur. The level is determined by the Gibbs free energy or equivalently, the reduction potential (E_f°), of the following reaction:

$$\mathrm{O} + \mathrm{e}^- \underset{k_b}{\overset{k_f}{\rightleftharpoons}} \mathrm{R}$$

As the electrode potential becomes more negative, i.e. more electrons populate the electrode surface, the formation of R will be favored (k_f increases), as described in Le Chatelier's principle. Therefore, the concentration of species O at the electrode surface decreases while that of R increases. However, the concentration does not change linearly because the

reaction is limited by diffusion, since only the molecules at the electrode surface undergo the reduction. Once the sweeping electrode potential reaches a set point E_v, it was swept back at the same rate. As the electrode potential goes to more positive value than E_f°, the formation of O is favored, because the electron population is taken away from the electrode[2].

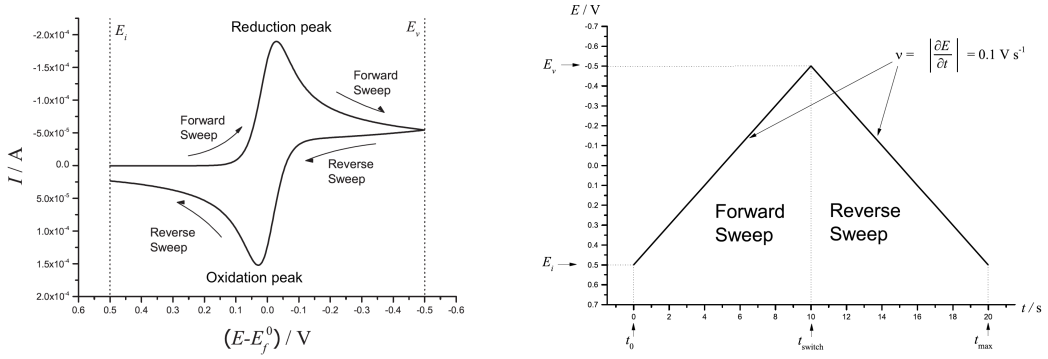

(a) A typical CV diagram produced by the application of the potential waveform in (b).

(b) The waveform of the potential applied during a typical cyclic voltammetry experiment.

Figure 1: Example of a CV diagram and the corresponding potential waveform [2].

During the entire CV process, a flux (or current) of species O and R develops at the electrode surface due to concentration gradient. A CV diagram records the flux as a function of the changed potential. During forward sweeping (E becomes more negative), O molecules diffuse toward the electrode surface where they are consumed and species R molecules diffuse away from the electrode surface where they are generated. The resulting peak flux (negative) is called the reduction peak. During backward sweeping (E becomes more positive), the diffusion processes in reverse directions take place. The resulting peak flux (positive) is called the oxidation peak. Note that figure1a reverses the direction of x- and y-axes but the CVs shown in later sections do not have the reversed axes.

According to Fick's first law, the flux j_{x_1} through a cross-section that is perpendicular to the diffusing axis x at point x_1 is

$$j_{x_1} = -D \left(\frac{\partial c}{\partial x} \right)_{x_1} \tag{1}$$

where D is the mass diffusivity of the diffusing species and c is the concentration of that

species. The time dependence of the concentration is described by Fick's second law:

$$\frac{\partial c}{\partial t} = D\left(\frac{\partial^2 c}{\partial x^2}\right) \tag{2}$$

For the simplest case, assume at the start of the CV process the concentration of species O is uniform everywhere:

$$c_O(x, t = 0) = c_O^*, \tag{3}$$

where c_O^* is the bulk concentration of species O. Also, assume the concentration of species R is zero everywhere at the beginning:

$$c_R(x, t = 0) = 0. \tag{4}$$

Define x as the distance away from the electrode surface. The spatial domain of the CV process is then $[0, x_{max}]$, where x_{max} is a sufficiently faraway distance from the electrode surface such that the concentration is not affected by diffusion. A typical value of x_{max} is equal to $6\sqrt{Dt_{max}}$, in which t_{max} is the maximum time the experiment will run for. The spatial boundary conditions of the CV process are given by

$$c(x = 0, t > 0) = f(E), \tag{5}$$

$$c(x = x_{max}, t > 0) = c^*. \tag{6}$$

Eq. 5 means that the concentration of each species at the electrode surface is dependent on the electrode potential. Eq. 6 describes that at distance sufficiently faraway from the electrode, the concentration is equal to the bulk concentration.[2][1]

We begin our simulation of the above system for the simplest situation: reversible chemical process with equal diffusion coefficients for the electroactive species. Using this model we screen several different numerical methods and schemes. The *Method Selection* section elaborates on our screening process.

Once the most accurate and least expensive numerical approximation is found, we move to simulate more complicated electrochemical processes, such as quasi-reversible and irreversible reactions, where electron transfer kinetics are slow (small k_f/k_b) with respect to diffusion rate and very asymmetric reactions, where a certain amount of perturbation in E initiates significantly different amount of change in k_f and k_b. By changing parameters

such as kinetic constant and transfer coefficient, which will be elaborated in *Simulating Quasi-reversible and Irreversible Electrochemical Reactions* section, the shape of CV diagram varies. We visualize how output results, such as peak positions and peak separations, change with respect to changing parameters by 3D and 4D plotting. Multi-threading reduces the computation time significantly.

In the end, we compare several simulated CV diagrams with an experimental CV and illustrate that a simulated CV can infer some properties of the electrochemical reaction.

Method Selection

A system of dimensionless parameters and coordinates is used throughout the computation for simplification. The following is a list of dimensionless parameters and their relation to physical quantities [2].

Parameter	Normalisation
concentration	$C_j = c_j / c_O^*$
diffusion coefficient	$d_j = D_j / D_O$
spatial coordinate	$X = x/\epsilon$
time	$T = D_O t/\epsilon^2$
potential	$\theta = (F/\mathcal{RT})(E - E_f^\circ)$
scan rate	$\sigma = (\epsilon^2/D_O)(F/\mathcal{RT})\nu$
current	$J = I/(\pi\epsilon F D_O c_O^*)$

where c_O^* is the bulk concentration of species O, D_O is the diffusion constant of species O, ϵ is the radius of the electrode, F is Faraday constant, $\mathcal{R}$ is the ideal gas constant, $\mathcal{T}$ is temperature in Kelvin and ν is the scan rate.

In dimensionless parameters, the one-electron reversible CV process with equal diffusion coefficients for the electroactive species is described by the partial differential equations

$$\frac{\partial C_O}{\partial T} = \frac{\partial^2 C_O}{\partial X^2} \tag{7}$$

$$\frac{\partial C_R}{\partial T} = \frac{\partial^2 C_R}{\partial X^2} \tag{8}$$

subject to initial and boundary conditions

$$\begin{aligned} C_O(X, T=0) = 1, \quad & C_R(X, T=0) = 0 \\ C_O(X = X_{max}, T > 0) = 1, \quad & C_R(X = X_{max}, T > 0) = 0 \\ C_O(X = 0, T > 0) = \frac{1}{1+e^{-\theta}}, \quad & C_R(X = 0, T > 0) = \frac{1}{1+e^{\theta}} \end{aligned}$$

where

$$X_{max} = 6\sqrt{T_{max}}$$

$$\begin{aligned} \theta &= \theta_i - \sigma T && \text{for } T \leq T_{max}/2 \\ \theta &= \theta_v + \sigma(T - \frac{T_{max}}{2}) && \text{for } T > T_{max}/2 \end{aligned}$$

Here T_{max} is the duration of a full period of forward sweep and backward sweep of the potential.[2]

We use finite difference method to numerically solve the system of partial differential equations. Note that we only need to solve the equation for species O because in this model the total concentration of two species at any X and T are the same, due to equal diffusion coefficients. Therefore the concentration of species R can be directly calculated as $C_R(X, T) = 1 - C_O(X, T)$. Below we use C to represent C_O for simplification.

First, we discretize C as C_i^k to approximate $C(i\Delta X, k\Delta T)$ and $i = 0, 1, \cdots n-1$, $k = 0, 1, \cdots, m-1$. Since we desire high accuracy and want to avoid time step constraint, we consider discretizing eq. 7 using central difference scheme (second order accurate) for the second derivative in space and using the backward Euler method (first order accurate) or the Crank-Nicolson method (second order accurate) for time evolution:

$$\text{(Backward Euler)} \quad \frac{C_i^{k+1} - C_i^k}{\Delta T} = \frac{C_{i-1}^k - 2C_i^k + C_{i+1}^k}{(\Delta X)^2} \tag{9}$$

$$\text{(Crank-Nicolson)} \quad \frac{C_i^{k+1} - C_i^k}{\Delta T} = \frac{C_{i-1}^k - 2C_i^k + C_{i+1}^k}{2(\Delta X)^2} + \frac{C_{i-1}^{k+1} - 2C_i^{k+1} + C_{i+1}^{k+1}}{2(\Delta X)^2} \tag{10}$$

Both methods are implicit, thus involving solving linear system. In the case of 1D, the system of equations is tridiagonal. For example, for the backward Euler method, the $n \times n$

linear system is given by

$$\begin{bmatrix} \beta_0 & \lambda_0 & & & \\ \alpha_1 & \beta_1 & \lambda_1 & & \\ & \ddots & \ddots & \ddots & \\ & & \alpha_{n-2} & \beta_{n-2} & \lambda_{n-2} \\ & & & \alpha_{n-1} & \beta_{n-1} \end{bmatrix} \begin{bmatrix} C_0^{k+1} \\ C_1^{k+1} \\ \vdots \\ C_{n-2}^{k+1} \\ C_{n-1}^{k+1} \end{bmatrix} = \begin{bmatrix} 1/(1+e^{-\theta}) \\ C_1^k \\ \vdots \\ C_{n-2}^k \\ 1 \end{bmatrix} \tag{11}$$

where for $i = 1, \cdots n-2$,

$$\alpha_i = -\frac{\Delta T}{(\Delta X)^2}, \quad \beta_i = 1 + 2\frac{\Delta T}{(\Delta X)^2}, \quad \gamma_i = -\frac{\Delta T}{(\Delta X)^2},$$

and for $i = 0, n-1$,

$$\alpha_i = 0, \quad \beta_i = 1, \quad \gamma_i = 0.$$

For tridiagonal system, efficient tridiagonal matrix algorithm (i.e. Thomas algorithm) can be used. The Thomas algorithm is a simplified version of Gaussian elimination, and works by alternately performing forward sweep and backward substitution on the solution vector, given pre-computed Thomas coefficients γ_i'. The complexity for the Thomas algorithm is $\mathcal{O}(n)$. For comparison, we also try the LAPACK banded solver.

The methods considered above all make use of evenly spaced grid points. In the simulation of electrochemical experiments, it is often beneficial to have adaptive spatial grid that provides more grid points near the electrode surface, where the changes in the concentration profile are more significant. Therefore, we use the exponentially expanding grids:

$$h_i = X_{i+1} - X_i = h\omega_X^i \tag{12}$$

where h is the distance between the first two grid points and ω_X is the expansion factor. With this adaptive spatial grid, the discretization formula needs to be modified. Using backward Euler method as an example,

$$\frac{C_i^{k+1} - C_i^k}{\Delta T} = \frac{\frac{C_{i+1}^k - C_i^k}{\Delta X_+} - \frac{C_i^k - C_{i-1}^k}{\Delta X_-}}{\frac{1}{2}\left(\Delta X_+ + \Delta X_-\right)} \tag{13}$$

where $\Delta X_+ = X_{i+1} - X_i$, $\Delta X_- = X_i - X_{i-1}$. The coefficients α_i, β_i, γ_i should also be modified accordingly.

The primary output results of the simulation is a series of computed flux at the surface electrode, which can be plotted as a CV diagram. We employ a three point discretization to approximate the flux:

$$\text{(even spatial grid)} \quad J^k = -\frac{-C_2^k + 4C_1^k - 3C_0^k}{2\Delta X} \tag{14}$$

$$\text{(adaptive spatial grid)} \quad J^k = -\frac{-C_2^k + (\omega_X + 1)^2 C_1^k - \omega_X(\omega_X + 2)C_0^k}{h\omega_X(\omega_X + 1)} \tag{15}$$

Below we show the error and complexity analyses of the different methods. The error is calculated based on the peak flux of a CV diagram (largest flux recorded during the forward sweep of potential). For a fully reversible electrode process, the peak flux is given analytically by $J_p = -0.446\sqrt{\sigma}$. Hence, after obtaining the simulated CV data, we find the peak flux and compute the relative error with respect to the analytic solution.

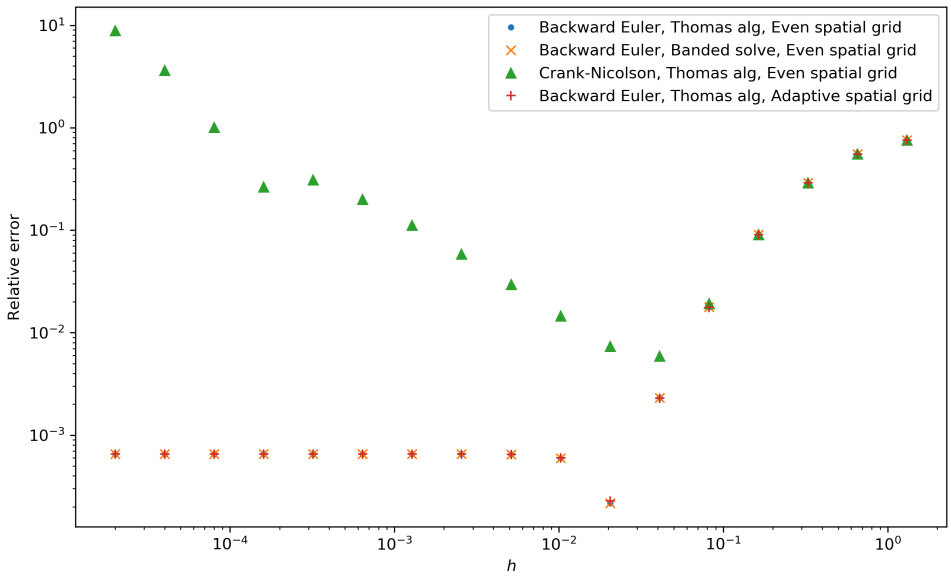

Figure 2: Relative error vs. grid spacing h for different methods (for adaptive spatial grid h is the spacing between the first two grid points).

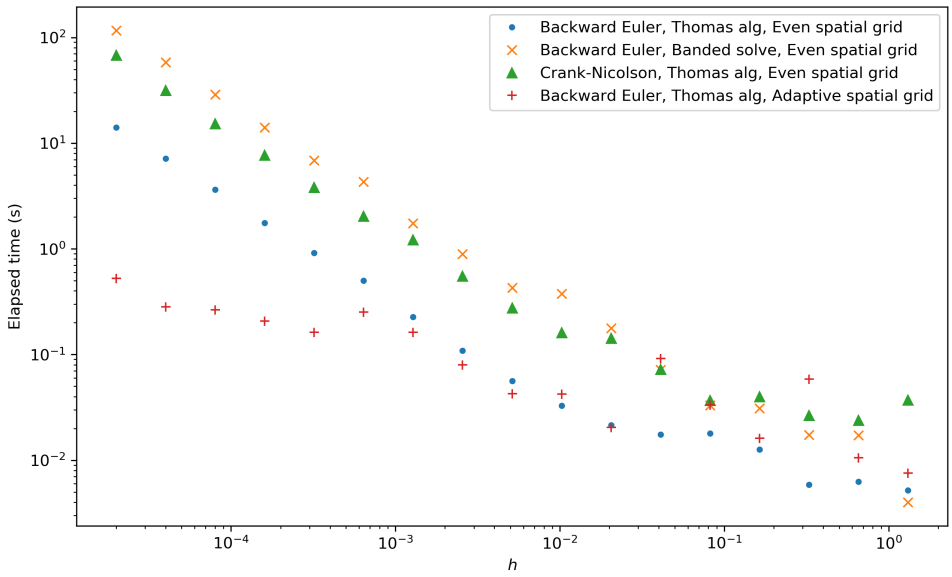

Figure 3: Elapsed time vs. grid spacing h for different methods (for adaptive spatial grid h is the spacing between the first two grid points).

According to figure 2, all methods converge to the analytic solution and share the same accuracy except for the Crank-Nicolson method solved by Thomas algorithm on even spatial grid. In theory Crank-Nicolson method is unconditionally stable. However, here we find that the simulated solution still contain oscillations when the ratio $\Delta T/(\Delta X)^2$ is large. The relative error for those converging methods stays constant when the grid spacing is small because the simulated peak flux has achieved the precision of the true value.

Figure 3 shows that the Thomas algorithm works much faster than the LAPACK banded solver, and the adaptive spatial grid reduces the computation time significantly at small grid spacings.

Therefore we conclude that in this experiment the backward Euler method with adaptive spatial grid solved by the Thomas algorithm is the method with least error and most efficiency.

Simulating Quasi-reversible and Irreversible Electrochemical Reactions

In this section, all simulations are performed using the aforementioned adaptive spatial grid and the Backward-Euler method with Thomas algorithm.

The CV diagram produced in last section is based on a reversible one-electron process, meaning that the reaction kinetics or electron transfer rate are much faster than diffusion rate and on the time scale of the experiment. In that case, the reduction-oxidation (redox) process is instantaneous compared to diffusion.

However, in reality, perfectly reversible reaction is rare and the equilibrium of species R and O can be sluggish. The flux, i.e. current, at the electrode surface can be written as:

$$J = -\left[k_f C_O(0,t) - k_b C_R(0,t)\right] \tag{16}$$

When species O and R are at equilibrium, there is an exchange current, which is caused by the dynamic process of O becoming R and R becoming O at the same rate. Such rate of the exchange process is described by the notation k^0 and its effect on the forward and backward reaction rate is described by the Butler-Volmer model as

$$k_f = k^0 e^{-\alpha\theta} \tag{17}$$

$$k_b = k^0 e^{(1-\alpha)\theta} \tag{18}$$

where α is the transfer coefficient, possessing value from 0 to 1 and θ is the dimensionless electrode potential. An α other than 0.5 means either the forward or the backward reaction is biased.

Several adjustments to the finite difference are made to accompany the introduction of kinetic and symmetrical influence. Eq. 16 can be expanded as a dimensionless expression

$$\left(\frac{\partial C_O(X,T)}{\partial X}\right)_0 = f(\theta)\frac{k^0\epsilon}{D}\left[C_R(0,T) - (1 + C_R^* - C_O(0,T))e^{\theta}\right] \tag{19}$$

where Butler-Volmer model expresses $f(\theta)$ as

$$f(\theta) = e^{-\alpha\theta} \tag{20}$$

A new dimensionless parameter κ^0 is introduced to account for the kinetics:

$$\kappa^0 = \frac{k^0\epsilon}{D} \tag{21}$$

κ^0 represents the ratio of exchange kinetic rate k^0 and diffusion rate D ($D = D_O = D_R$). On a fixed electrode surface, large κ^0 (> 100) means electron transfer process is much faster than diffusion and hence a reversible CV diagram will form. if κ^0 is small ($< 10^{-2}$), the resulting CV diagram will have huge peak separation and hence irreversible behavior. Discretizing eq. 19, the surface concentration influenced by kinetics is the new upper boundary condition and is expressed as

$$C^k_{O,0} = \frac{hf(\theta)\kappa^0(1 + C^*_R)e^\theta + C^k_{O,1}}{1 + hf(\theta)\kappa^0(1 + e^\theta)} \tag{22}$$

where h is the grid size of the first interval. Since the surface concentration $C^k_{O,0}$ is now dependent on $C^k_{O,1}$, $C^k_{O,0}$ must be solved within the Thomas algorithm. This is achieved by setting at each iteration

$$\begin{aligned}
\alpha_0 &= 0 \\
\beta_0 &= 1 + hf(\theta)\kappa^0(1 + e^\theta) \\
\gamma_0 &= -1 \\
C^k_{O,0} &= hf(\theta)\kappa^0 e^\theta
\end{aligned}$$

As these surface coefficients vary with time development, the Thomas coefficients γ'_i are no longer set constant, but instead updated within the time-evolving-loop. The CV diagrams generated using different κ^0 and α with $C^*_R = 0$ are shown and compared. Note that our generated CV diagrams will look different from the typical diagram shown in figure 1a, in that we keep the axes in original directions. In such case, the oxidation peak is at the top, and the reduction peak is at the bottom.

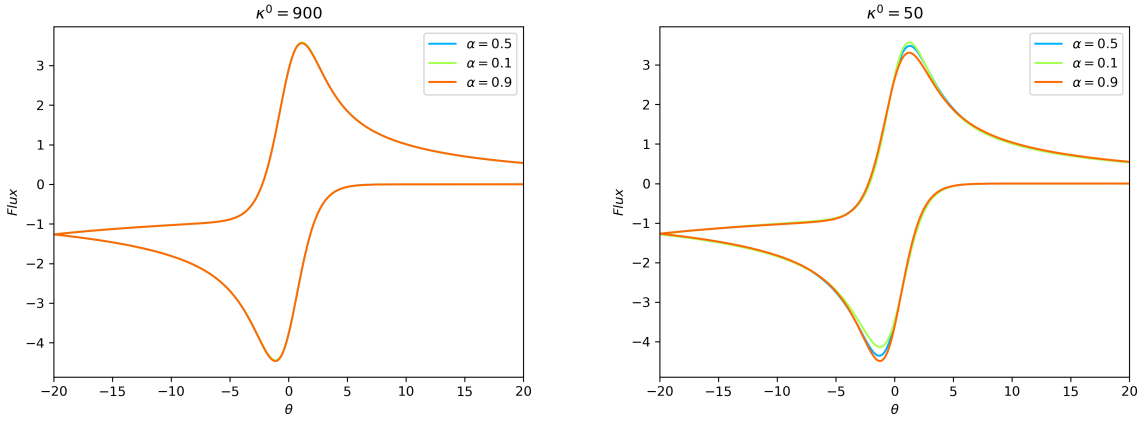

(a) $\kappa^0 = 900$ (b) $\kappa^0 = 50$

Figure 4: CV diagrams of completely reversible (a) and reversible-like-quasireversible (b) reactions

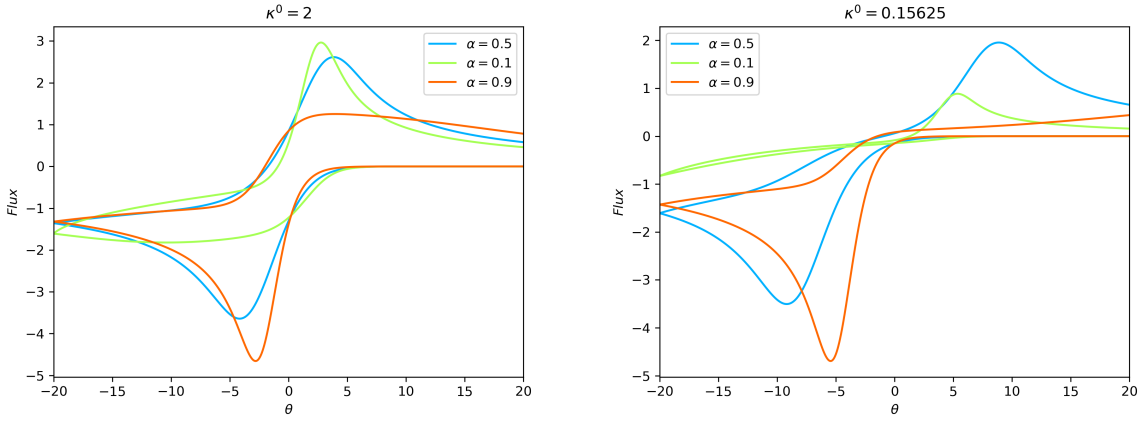

(a) $\kappa^0 = 2$ (b) $\kappa^0 = 0.15625$

Figure 5: CV diagrams of irreversible-like-quasireversible (a) and completely irreversible (b) reactions

We first study the effect of transfer coefficient α by setting κ^0 constant. Other parameters are also set constant. We use four different values of κ^0, 900, 50, 2 and 0.15625, which refer to completely reversible, reversible-like-quasireversible, irreversible-like-quasireversible and completely irreversible cases, respectively. In figure **??**(a), the kinetic rate constant is so large that α within the range of $[0.1, 0.9]$ has minimal effect on the shape of CV. This is

evident from eq. 19. As kinetic constant becomes smaller and diffusion's effect starts to take over, difference in α will completely change the shape of CV. In quasireversible cases (figure **??**(b) and figure **??**(a)), a large α increases $\frac{J_{red}}{J_{ox}}$ (the ratio between the reduction peak flux and the oxidation peak flux) while a small α decreases the ratio. In the irreversible case (figure **??**(b)), no oxidation peak is observed when α is large and no reduction peak is observed when α is small.

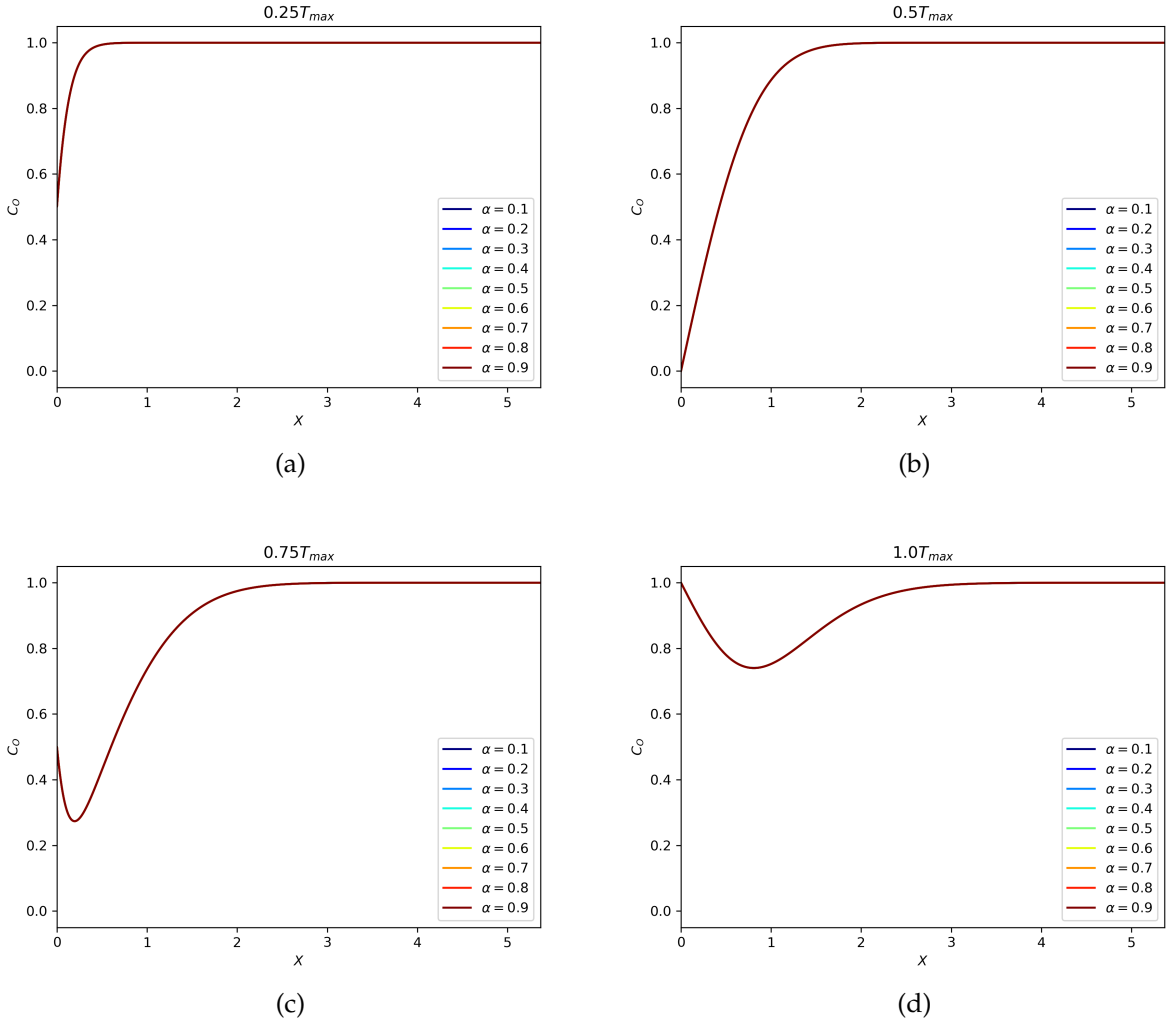

(a) (b)

(c) (d)

Figure 6: Concentration profile of species O at different T for $\kappa^0 = 900$

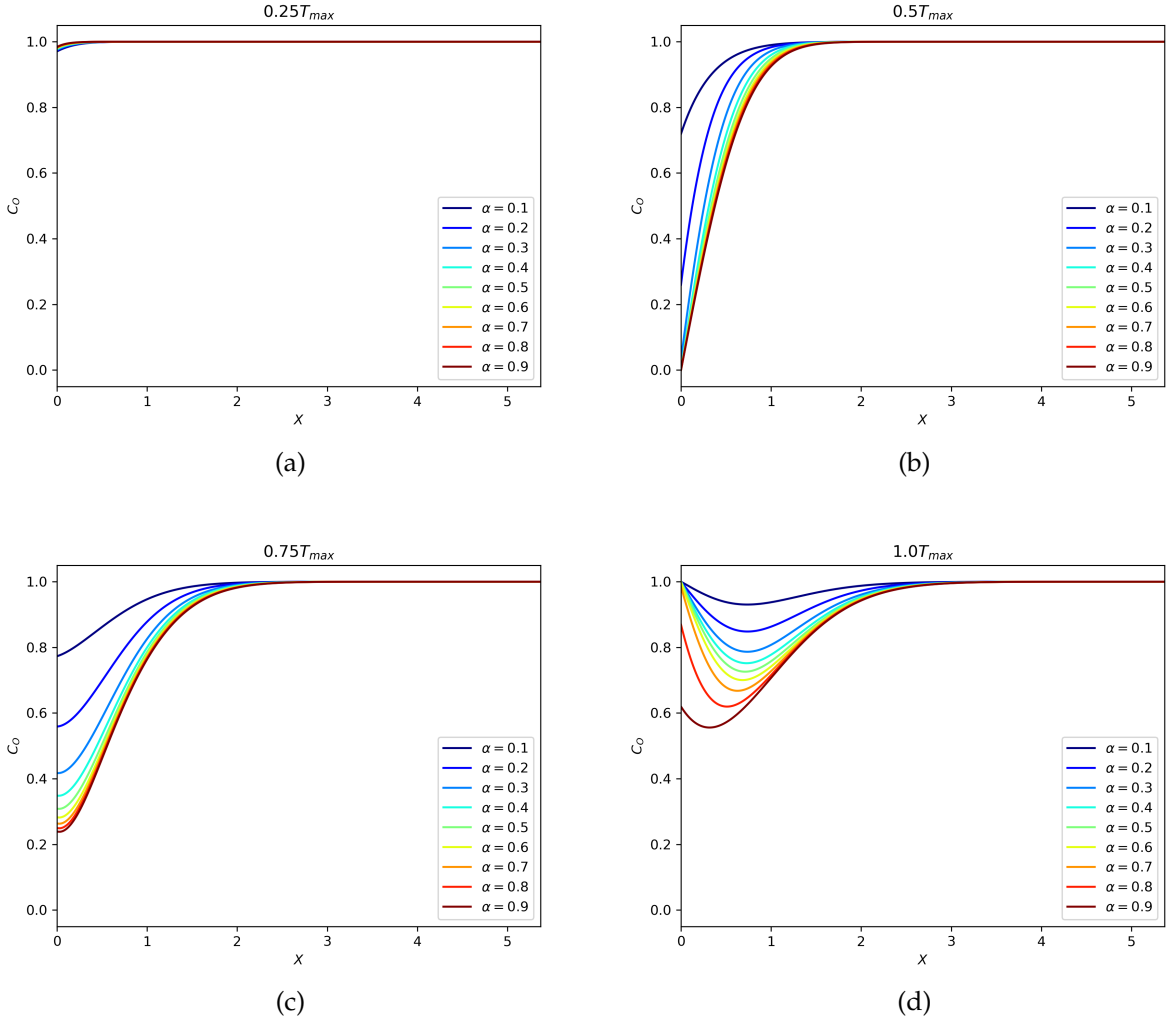

(a) (b)

(c) (d)

Figure 7: Concentration profile of species O at different T for $\kappa^0 = 0.15625$

The concentration profile of a completely reversible process is uninfluenced by changing α while the reaction with sluggish kinetics has a very different concentration profile due to different α. At $0.25T_{max}$, the surface concentration in the reversible process (figure 6) is only around 60% of the bulk solution, while the sluggish kinetics(figure 7(a)) of the irreversible reaction hinder the concentration change. In the irreversible process, the change in concentration of species O is trivial for $\alpha = 0.1$ compared with the concentration change with $\alpha = 0.9$. This phenomenon reflects eq. 17, eq. 18 and the chemical equation shown in the beginning. Smaller α makes it very hard to increase k_f by changing θ, which results a favorable condition for species O to be present in solution while. This is

exactly the opposite for species R, an easily enlarged k_b keeps converting R to O. A more quantitatively presented result will be shown later.

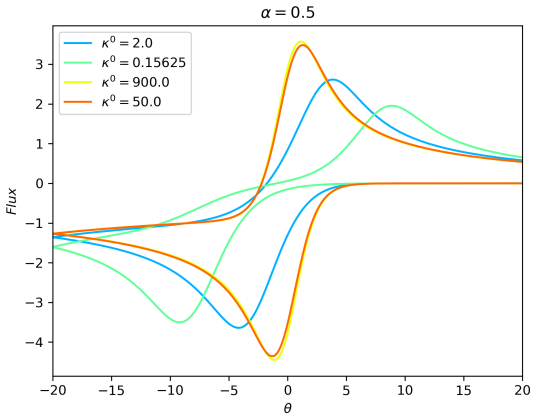

(a) $\alpha = 0.5$

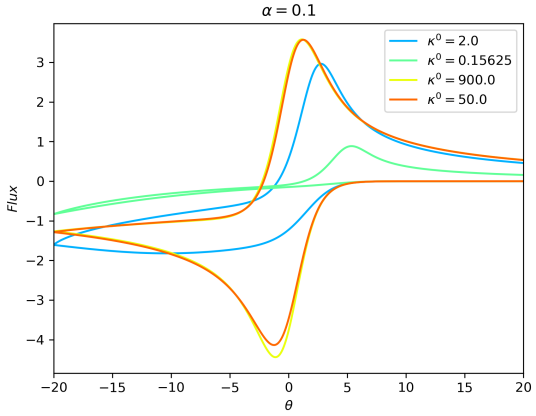

(b) $\alpha = 0.1$

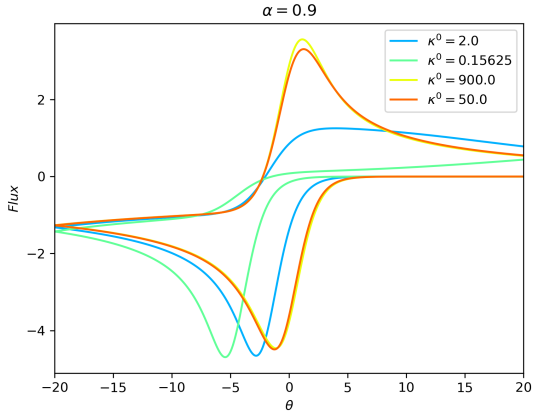

(c) $\alpha = 0.9$

Figure 8: CV diagrams of different transfer coefficient α.

The effects of κ^0 or similarly k^0 are studied by setting α and other parameters constant. Figure 8(a) shows the most important effect of decreasing κ^0: increasing the separation between E_{red} and E_{ox}. This reveals that when reaction kinetics is small, much of the energy carried by electrons is consumed for activating the reaction, in either direction. In a battery charging process, if κ^0 is small, less energy will be stored in a battery than energy input. During discharging process, less energy will be acquired by electrics than the battery actually delivers. For the irreversible process $\kappa^0 = 0.15625$, small α gives very tiny oxidation peak while large α gives huge reduction peak. This is caused by the fact that

the flux in oxidation process is a measure of how fast species R converts to O. However, with a bias toward O caused by the small α, very small amount of R is generated, so the conversion of R to O is minimal, which causes a small flux.

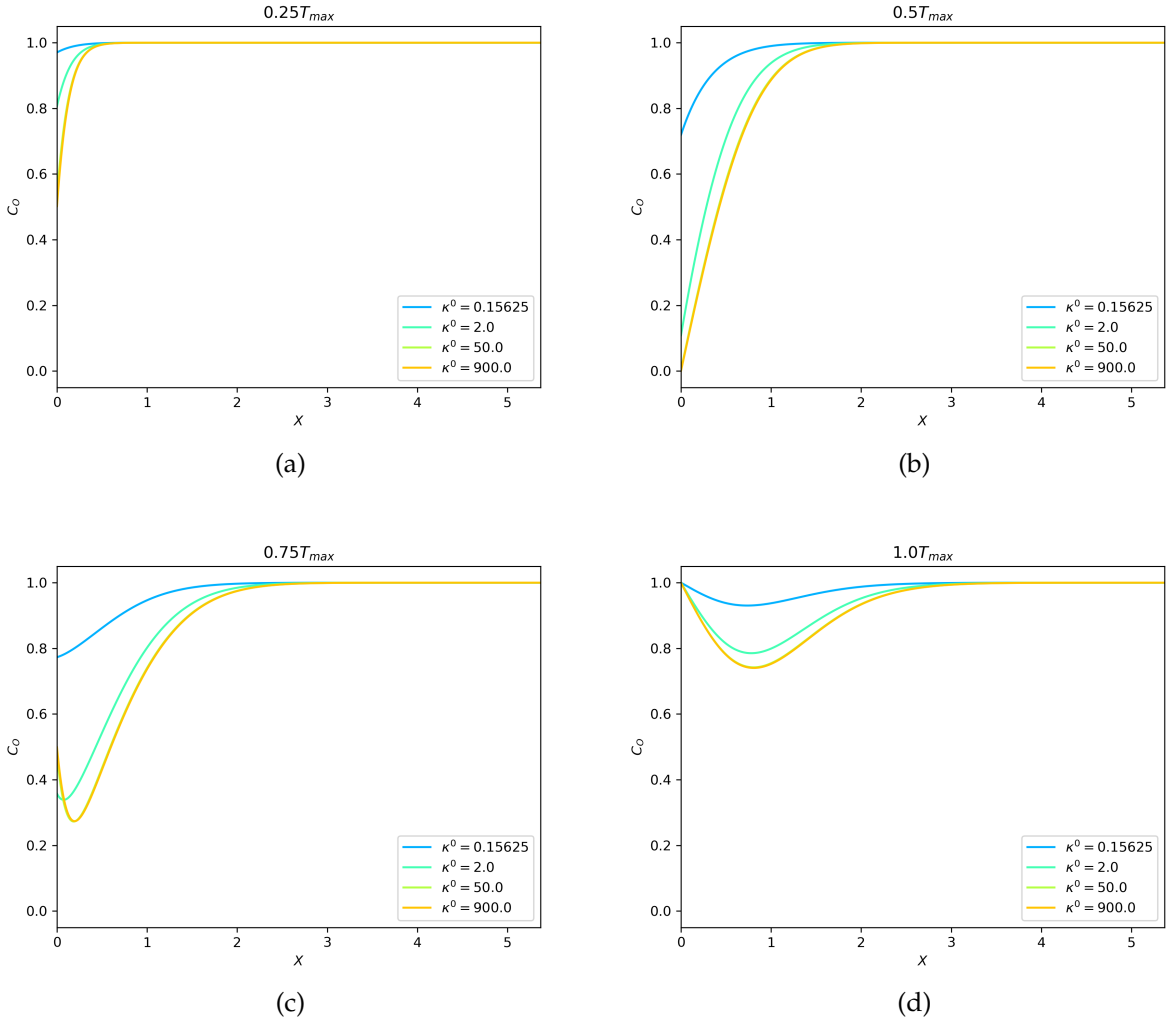

Figure 9: Concentration profile of species O at different T for $\alpha = 0.1$

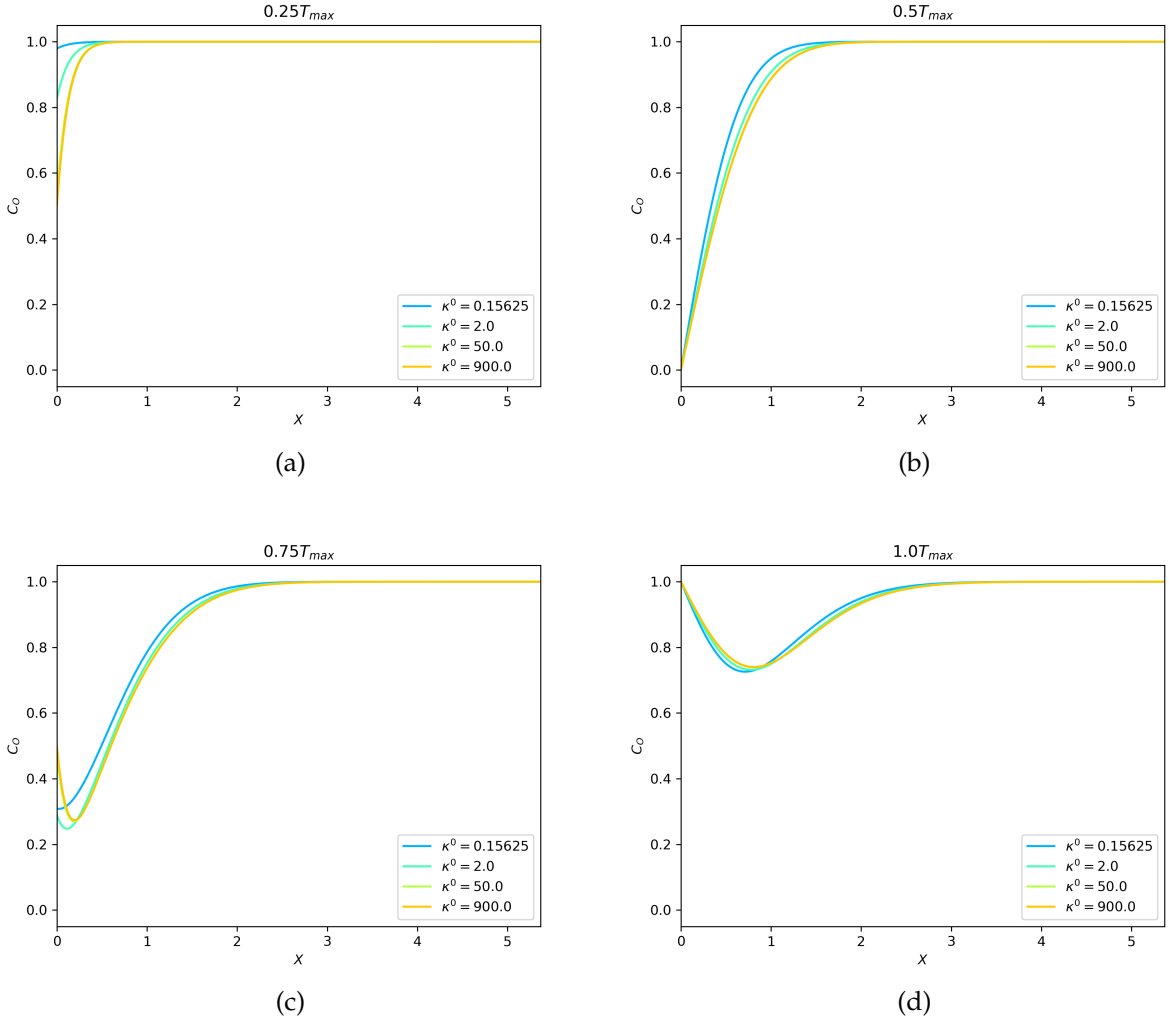

Figure 10: Concentration profile of species O at different T for $\alpha = 0.5$.

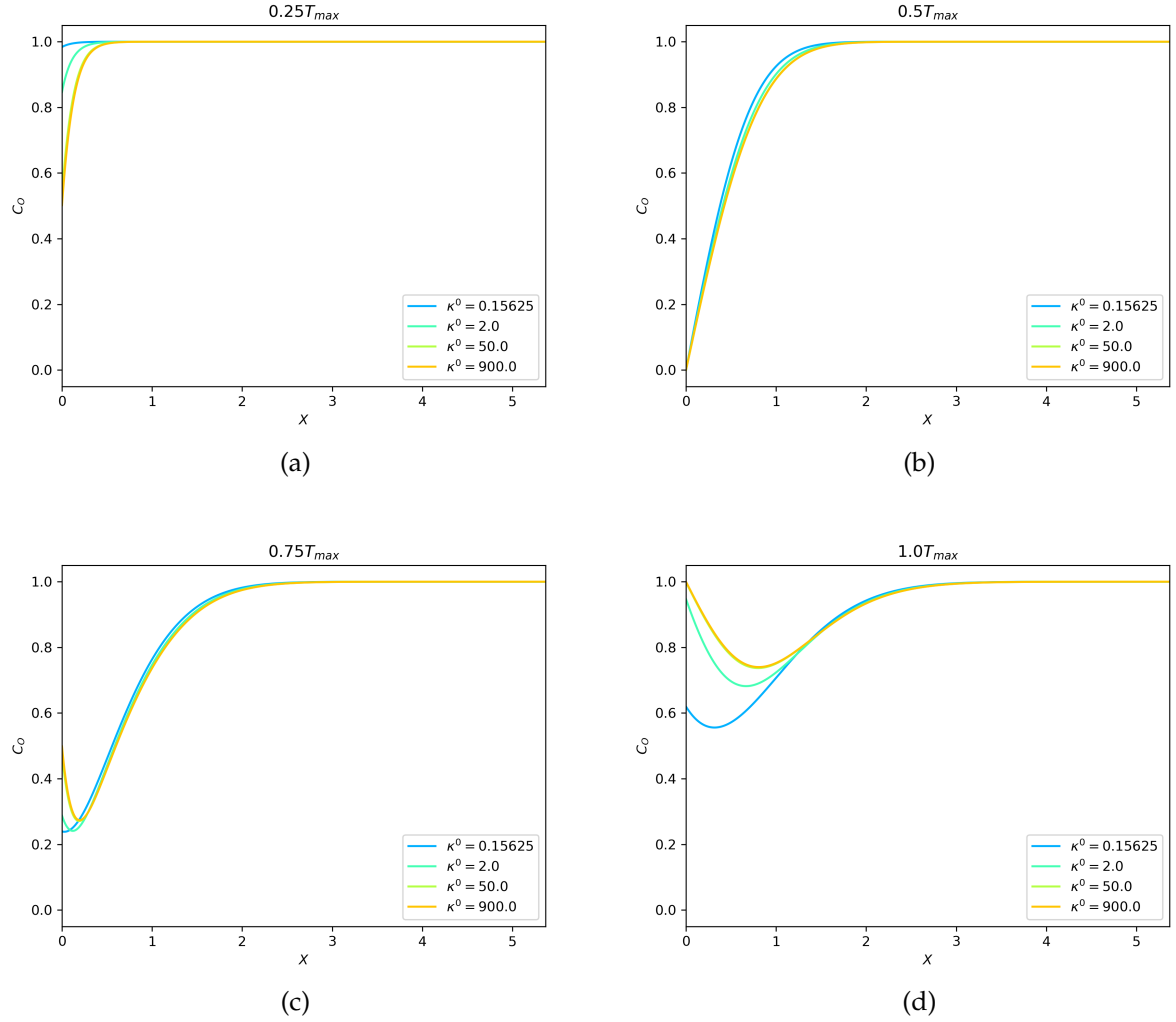

Figure 11: Concentration profile of species O at different t for $\alpha = 0.9$

At $\alpha = 0.5$, the concentration profile of the most irreversible case is always above other curves(figure 10(a)(b)(c), most evident in (a)), indicating a drag in concentration change. However, regardless of the drag, at T_{max}, the concentration profiles are quite similar, reflecting the fact that within this range of κ^0 and an $\alpha = 0.5$, the thermodynamic property is maintained. On the contrary, at extreme α values (figure 9 and figure 11), not only the kinetic difference appears, but also thermodynamic difference is observed at the experiment timescale. At $T = \infty$, the concentration of all κ^0 will converge to 1.

As shown in the above examples, varying κ^0 and α alters the shape of CV diagram. To be more specific, they change the location, i.e. θ, of the reduction and the oxidation

peak as well as the intensity, i.e. flux, of the peaks. The dependence of reduction peak flux (figure 12(a)), oxidation peak flux (figure 12(b)), reduction peak θ (figure 13(a)), oxidation peak θ (figure 13(b)) and peak separation (figure 14(a)) on α and κ^0 is presented in the following figures.

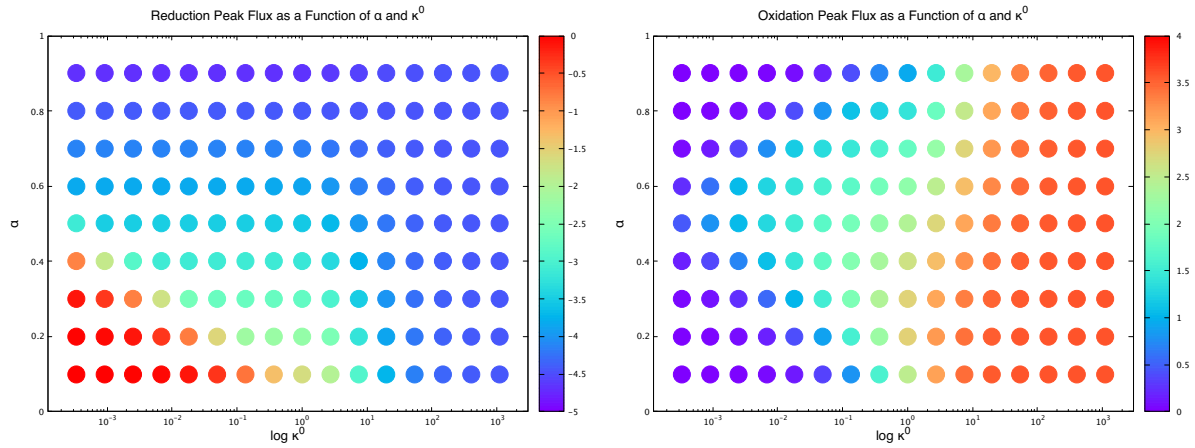

(a) Reduction Peak Flux (b) Oxidation Peak Flux

Figure 12: The dependence of peak flux on κ^0 and α

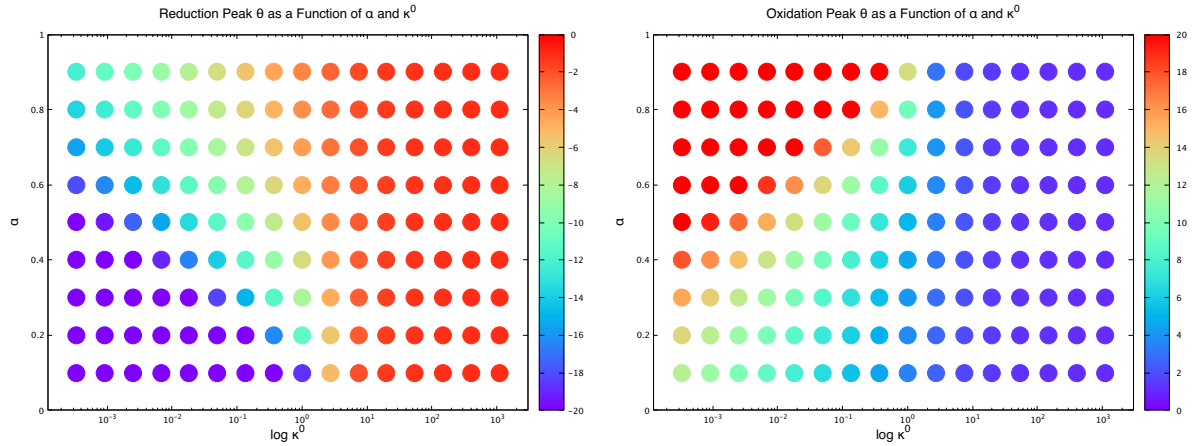

(a) Reduction Peak θ (b) Oxidation Peak θ

Figure 13: The dependence of peak θ on κ^0 and α.

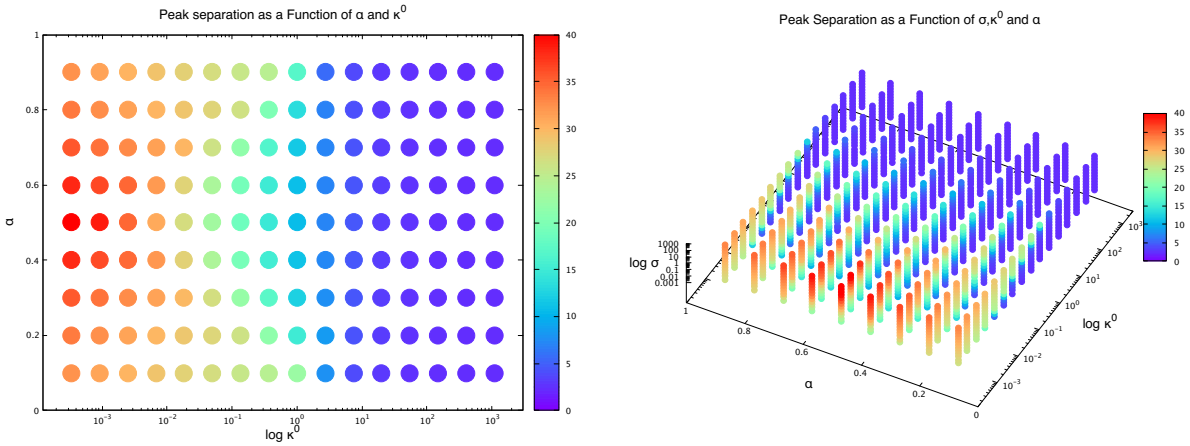

(a) Peak Separation

(b) Peak Separation Dependence on κ^0, α and σ

Figure 14: Peak separation dependence on α and κ^0(a) and σ(b)

Figure 12(a) indicates that at small κ^0 and small α, the reduction peak disappears and figure 12(b) shows a 0 oxidation peak at small κ^0 for both large and small α, which is caused by the reason explained previously. The rightmost column of figure 13(a) and (b) reveals a negligible effect of α when κ^0 is large. This phenomenon is more clearly presented in figure 14(a), which points out the peak separation only varies at small κ^0. Besides α and κ^0, the scan rate σ is another parameter that affects peak intensity and position and its effect is illustrated in figure 14(b). Again, at large κ^0, neither α nor σ can affect peak properties.

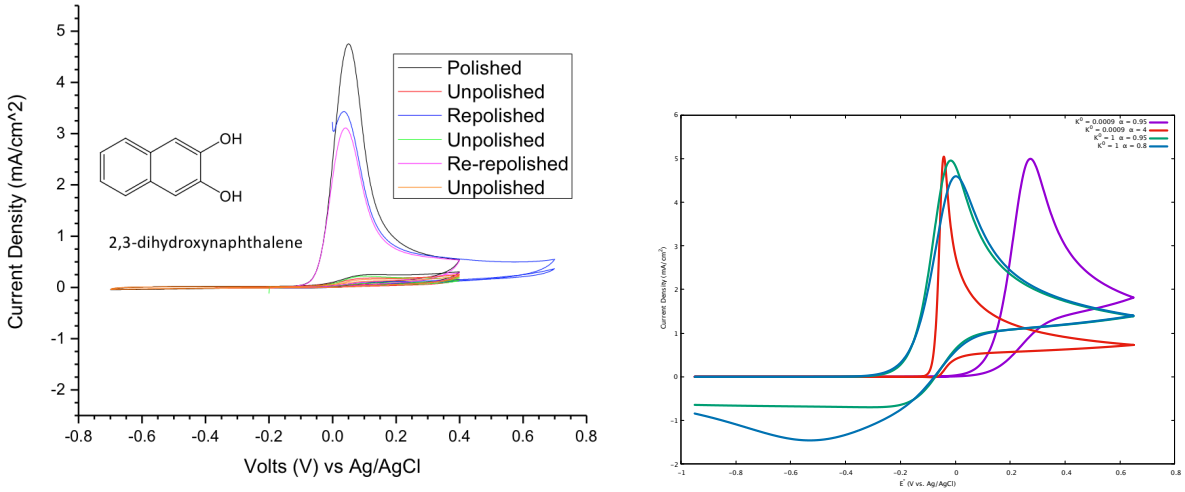

(a) CV of 2,3-dihydroxynaphthalene

(b) Simulated CV

Figure 15: The experimental CV of 2,3-dihydroxynaphthalene (a) and several simulated CVs(b)

The CV of 2,3-dihydroxynaphthalene (figure 15(a)) has been previously experimentally taken by Dr.Michael R. Gerhardt, a former graduate from Prof. Michael Aziz's group at SEAS. We attempt to simulate this CV by changing α, κ^0 and some scaling. In the simulated CVs(figure 15(b)), the blue curve and the green curve have a large κ^0 and show non-zero flux at negative E, which is inconsistent with the actual CV, so we know the true kinetics must be even smaller. The red and violet curves both appear to be similar to the experimental data but the red one captures the curvature more precisely. However, the red curve is un-physical since α should only have value in between 0 and 1. Several other conditions have not been included in the simulation. For example, the oxidation of 2,3-dihydroxynaphthalene is a two-electron process while the simulator only considers one. Since we do not know what scan rate Dr. Gerhardt used to obtain the CV, we need to vary scan rate to see the difference, too. In addition, the oxidation of 2,3-dihydroxynaphthalene may incur chemical decomposition, which is not considered in the Thomas algorithm. We can improve the CV simulator by taking into account two-electron process and chemical degradation. If the experimental setup of CV is fully known, comparing the simulated CV and an experimental CV may give important information of the properties, such as α and κ^0 of the species being tested.

Conclusion

We aim to simulate cyclic voltammetry experiments using finite difference methods. An implicit scheme is used and we compare the accuracy and efficiency of different methods (backward Euler method, Crank-Nicolson method and backward Euler method with adaptive spatial grid) and linear solvers (Thomas algorithm and LAPACK banded solver). We find the backward Euler method with adaptive spatial grid solved by Thomas algorithm to be the most accurate and efficient method, so we proceed to simulations using this method. By simulating CVs with varying κ^0, α and σ we generate a series of 2D maps and a 3D map showing how CV properties change with these parameters. An experimental CV of 2,3-dihydroxynaphthalene is compared with several simulated CVs. Without knowing the actual k^0 of the reduxtion-oxidation reaction for this molecule, the simulated CVs inform the k^0 should be sufficiently small compared with the molecule's diffusion constant. The imperfection of the simulated CVs also indicated potential improvements, such as including degradation kinetics and multiple electron process, to the simulator. The upgraded CV simulator should be able to generate all different shapes of CV and reveal to electrochemists the important properties of the reaction they are interested. This will be essential in understanding the behavior of batteries, material corrosion and other electrochemical phenomena.

References

[1] A. J. Bard, L. R. Faulkner, Electrochemical Methods Fundamentals and Applications, John Wiley and Sons., Inc., 2001.

[2] R. G. Compton, E. Laborda, K. R. Ward, Understanding voltammetry: simulation of electrode processes, World Scientific, 2014.